

# Supersymmetric dark matter in M31: can one see neutralino annihilation with CELESTE?

October 7th, 2002  
preprint GAM-2002/03  
preprint LAPTH-937  
preprint PM/02-03

A. Falvard, E. Giraud, A. Jacholkowska, J. Lavalley, E. Nuss, F. Piron,  
and M. Sapinski<sup>1</sup>

*Groupe d'Astroparticules de Montpellier, UMR5139-UM2/IN2P3-CNRS, Place Eugène  
Bataillon - CC85, 34095 Montpellier, France*

P. Salati and R. Taillet

*Laboratoire de Physique Théorique LAPTH, Annecy-le-Vieux, 74941, France and  
Université de Savoie, Chambéry, 73011, France*

K. Jedamzik and G. Moultağa

*Laboratoire de Physique Mathématique et Théorique, UMR5825-UM2/CNRS, Place  
Eugène Bataillon, 34095 Montpellier Cedex 5, France*

## Abstract

It is widely believed that dark matter exists within galaxies and clusters of galaxies. Under the assumption that this dark matter is composed of the lightest, stable supersymmetric particle, assumed to be the neutralino, the feasibility of its indirect detection via observations of a diffuse gamma-ray signal due to neutralino annihilations within M31 is examined. To this end, first the dark matter halo of the close spiral galaxy M31 is modeled from observations, then the resultant gamma-ray flux is estimated within supersymmetric model configurations. We conclude that under favorable conditions such as the rapid accretion of neutralinos on the central black hole in M31 and/or the presence of many clumps inside its halo with  $r^{-3/2}$  inner profiles, a neutralino annihilation gamma-ray signal is marginally detectable by the ongoing collaboration CELESTE.

---

<sup>1</sup>on leave from Henryk Niewodniczanski Institute of Nuclear Physics in Cracow

# 1 Introduction

The existence of cosmic dark matter is required by a multitude of observations and arguments, such as the excessive peculiar velocities of galaxies within clusters of galaxies or gravitational arcs, indicating much deeper gravitational potentials within clusters than those inferred to be present from only the luminous matter content. Also an epoch of Big Bang nucleosynthesis predicts a fractional contribution of baryons to the critical density,  $\Omega_b$ , significantly smaller than the total  $\Omega$  in form of clumpy matter inferred to exist from observations of large-scale galactic peculiar velocities (e.g.,  $\Omega \approx 0.3$ ). Establishing the nature of the dark matter is one of the outstanding problems and challenges in cosmology. Virtually all proposed candidates require physics beyond the standard model of particle physics. A candidate particularly well-suited to the formation of the observed large-scale structure, is a weakly interacting particle with comparatively small velocities before the onset of structure formation (i.e. cold dark matter, hereafter CDM).

Due to the small thermal velocity of CDM, fluctuations survive from the early universe on all scales. CDM is a bottom up scenario in which structures develop as small clumps collapse and undergo series of merging resulting in the hierarchical formation of massive dark matter halos. These halos are the hosts of baryonic systems, from galaxies to clusters, which cooled and condensed by dissipating energy. Cosmological N-body simulations describe well this non-linear complex series of mergers, accretion events and violent relaxation which are in general agreement with observations but are subject to some difficulties on galactic scales. An overview of these issues was recently presented by [1]. It remains to be seen if the discrepancies on small scales may be solved by the particulars of baryonic physics (e.g. star formation, feedback, galactic black holes), or if indeed, the paradigm of cold dark matter is being challenged. In contrast, the excellent performance of cold dark matter (with initial adiabatic, scale-invariant density perturbations) on large scales seems still undiminished.

On the particle physics side, supersymmetric models are believed to provide the most promising approach to physics beyond the standard model. Supersymmetry can cure in principle several conceptual shortcomings of this model, although definitively compelling scenarios are still to come. Of interest for us here is the prediction of, as yet undetected, bosonic particles for each fermionic standard model particle, and vice versa, expected to lie in the approximate mass range of  $\sim 100\text{GeV} - 1\text{TeV}$  which are actively searched for at present and future colliders. In particular, the lightest supersymmetric particle (LSP), under the assumption of its stability (R-parity conservation) or at least quasi stability on the cosmological time scale, may serve as the dark matter particle as long as it is neutral

(i.e. a neutralino). Moreover, its interactions are believed such that it would behave as CDM, and its relic abundance may be naturally of order  $\Omega \sim 1$  within the minimal supersymmetric extension of the standard model (MSSM), for review see [2]. This is of course a very exciting possibility.

There is a large number of ongoing underground experiments attempting to detect neutralinos within the solar system by "direct" scattering on nuclei. An alternative approach for the detection of neutralinos is via their occasional annihilation in dark matter halos, and observation of the resultant gamma-rays (and/or neutrinos). However, when it comes to quantitative predictions in relation to experimental detection, one has to tackle with astrophysical uncertainties such as the halo modelling of the astrophysical object under consideration, as well as with particle physics uncertainties related to our ignorance of the physics underlying supersymmetry breaking. The possible detection of such a gamma-ray signal from the spiral galaxy M31 (Andromeda), at a distance of 700kpc, is the subject of the present paper. We will deal mainly with two complementary issues: (i) we give different models of the dark halo component in addition to the disk and bulge components previously studied in the literature; (ii) assuming this dark matter is accounted for by the lightest neutralino of the MSSM, we analyse the gamma-ray fluxes that can originate from the pair annihilation of these particles, in terms of model assumptions such as minimal supergravity.

The paper is organized as follows: section 2 is devoted to M31 halo modelling. In section 3 we first recall briefly the basic ingredients and tools we use for the study of the supersymmetric dark matter signature and then present the main predictions. Section 4 explores the discovery potential of the CELESTE experiment. Section 5 is devoted to a quantitative discussion of possible signal enhancement due to clumpiness and black hole presence in M31.

## 2 Modeling the neutralino halo around M31

### 2.1 Rotation curve of M31 without dark halo

The late-type Sb spiral galaxy M31 lies at a distance of 700 kpc . The visible part mostly consists of a bulge and a disk. The present analysis is based upon the investigation of the neutral hydrogen content of M31, and the model-independent derivation of the velocity field, performed by Braun [3]. The rotation curve, after correction for the ellipticity which the spiral exhibits in the inner 5 kpc, is well fitted with two mass components which are both traced by optical observations: (i) A bulge – with total mass  $7.8 \pm 0.5 \times 10^{10} M_{\odot}$

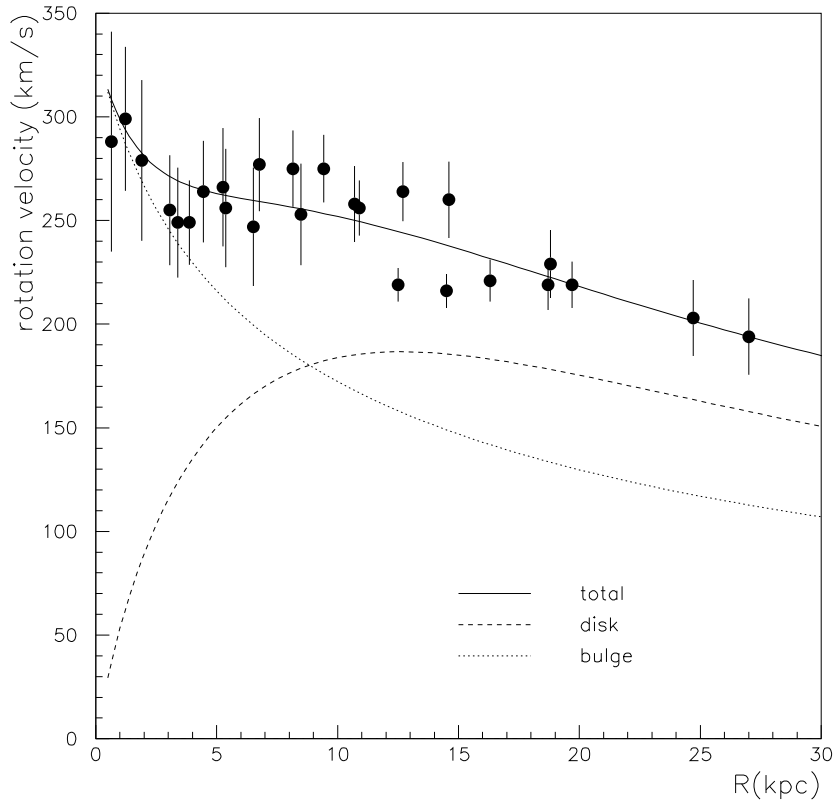


Figure 1: the rotation velocity data points of the spiral Sb galaxy M31 are well fitted by the two-component model discussed in [3]. The mass-to-light ratios – in the blue band – of the bulge and the disk – dotted curves – are respectively  $\Upsilon_{bulge} = 6.5 \pm 0.4 \Upsilon_{B,\odot}$  and  $\Upsilon_{disk} = 6.4 \pm 0.4 \Upsilon_{B,\odot}$ . This leads to the global rotation solid curve. Note that  $\Upsilon_{disk}$  is too large to be consistent with the young stars that populate the disk.

– and assuming a mass-to-light ratio of  $\Upsilon_{bulge} = 6.5 \pm 0.4 \Upsilon_{B,\odot}$  where  $\Upsilon_{B,\odot}$  is the mass-to-light ratio for the Sun. This value may be compared to the limit of  $3.7 \leq \Upsilon_{bulge} \leq 5.7$  that has been derived from synthetic stellar models [4] assuming the same bulge color and a population age lying in the range from 9.5 Gyr to 15.5 Gyr; (ii) The disk with a mass of  $1.22 \pm 0.05 \times 10^{11} M_{\odot}$  in the inner 28 kpc.

These contributions of the disk and the bulge components to the rotation curve are plotted in Fig. 1. Note that this figure reproduces Fig. 8b of [3]. Braun concludes that no dark halo is necessary to account for the velocity field inside M31. This result relies, nevertheless, on the crucial assumption that the mass-to-light ratio of the disk is  $\Upsilon_{disk} = 6.4 \pm 0.4 \Upsilon_{B,\odot}$ . Such a large value does not agree with estimates based on the blue color

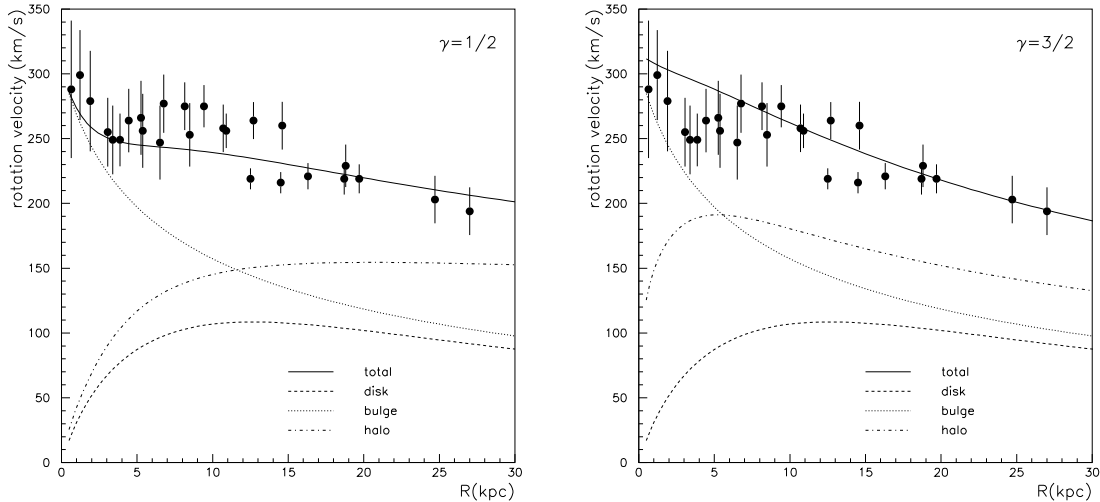


Figure 2: a massive halo has been assumed in both plots by taking small yet plausible values for the mass-to-light ratios of the bulge –  $\Upsilon_{bulge} = 3.5 \Upsilon_{B,\odot}$  – and of the disk –  $\Upsilon_{disk} = 2.5 \Upsilon_{B,\odot}$ . The left pannel corresponds to a value of  $\gamma = 1/2$  for the halo mass density singularity near the center whereas the right panel features the case of a Moore’s profile with  $\gamma = 3/2$ . In both cases, the observations are not well reproduced by the global rotation – solid – curves.

of the disk and on synthetic spectra of young stellar populations which it contains [4]. The mass-to-light ratio  $\Upsilon_{disk}$  of a purely stellar component should actually not exceed  $\sim 3.8 \Upsilon_{B,\odot}$ . In addition, a disk as massive as that proposed by Braun should generally be unstable. We therefore feel that Braun has overestimated the importance of the disk so that a halo around M31 is indeed a viable possibility.

## 2.2 Rotation curve of M31 including a dark halo

Since a disk and a bulge may not be enough to model the rotation velocity of M31, we have assumed the presence of an additional mass component in terms of a spherical halo whose mass density profile is generically given by

$$\rho_\chi(r) = \rho_0 \left( \frac{r_0}{r} \right)^\gamma \left\{ \frac{r_0^\alpha + a^\alpha}{r^\alpha + a^\alpha} \right\}^\epsilon . \quad (1)$$

A cored isothermal profile with core radius  $a$  corresponds to  $\gamma = 0$ ,  $\alpha = 2$  and  $\epsilon = 1$ . A NFW profile [5] is obtained with  $\gamma = 1$ ,  $\alpha = 1$ , and  $\epsilon = 2$ , whereas Moore’s distribution [6] is recovered if  $\gamma = \epsilon = 3/2$  and  $\alpha = 1$ . For a given halo profile our mass models have two free parameters: the mass-to-light ratio of the disk and that of the bulge. While there

is ample freedom on the relative importance of the disk and the halo, the observations set stringent constraints on the structure of the neutralino halo and actually favours a NFW [5] distribution. This is illustrated in Fig. 2 where the central singularity of the neutralino density has been set equal to  $\gamma = 1/2$  (left panel) and  $\gamma = 3/2$  (right panel). The contributions of the bulge and the disk correspond to the dotted and dashed curves, respectively, whereas the dashed-dotted lines denote the halo. The global rotation – solid – curves fail to match the observation points for medium range of  $R$  (a) and below 5 kpc (b). We have therefore disregarded these profiles in what follows and have concentrated on the NFW ( $\gamma = 1$ ) case. This is not surprising insofar as a  $1/r$  spherical profile leads to the same rotation curve as a disk with constant surface mass density.

The neutralinos potentially concealed around M31 should annihilate and produce high-energy photons. The corresponding flux at Earth,  $n_\gamma$  – per unit of time, surface, and solid angle – may be expressed as

$$\frac{dn_\gamma}{dt dS d\Omega} = \frac{1}{4\pi} \frac{\langle\sigma v\rangle N_\gamma}{m_\chi^2} \int_{\text{los}} \rho_\chi^2 ds = \frac{1}{4\pi} \frac{\langle\sigma v\rangle N_\gamma}{m_\chi^2} \mathcal{J}(R) \quad (2)$$

where  $m_\chi$  is the neutralino mass and  $\langle\sigma v\rangle N_\gamma$  denotes the thermally averaged annihilation rate yielding  $N_\gamma$  gamma-rays in the final state. The astrophysical part of the expression consists in the integral  $\mathcal{J}$  along the line of sight of the neutralino density squared  $\rho_\chi^2$ . Assuming a spherical halo with radial extension  $R_{\text{max}}$  leads to

$$\mathcal{J}(R) = 2 \int_0^{\sqrt{R_{\text{max}}^2 - R^2}} \rho^2(\sqrt{s^2 + R^2}) ds , \quad (3)$$

for a direction with impact parameter  $R$  off the centre of M31. Because the density decreases steeply at large distances (see Eq. 1), our results are not sensitive to the actual value of the radial cut-off  $R_{\text{max}}$ . The next step is the sum of the line of sight integral  $\mathcal{J}$  over the solid angle subtended by the source

$$\Sigma = \int \mathcal{J}(R) d\Omega . \quad (4)$$

We are interested in the number  $I_\gamma$  of high-energy photons – collected per unit of time and surface – that originate from a circular region with angular radius  $\theta_{\text{obs}}$ . The previous expression simplifies into

$$\Sigma = 2\pi \int_0^{\theta_{\text{obs}}} \mathcal{J}(R) \sin\theta d\theta , \quad (5)$$

where  $R/D = \tan\theta \simeq \theta$  and  $D \sim 700$  kpc is the distance to M31. Integrating relation (2) over the source leads to the gamma-ray signal

$$I_\gamma = \left(3.18 \times 10^{-13} \text{ photons cm}^{-2} \text{ s}^{-1}\right) \left\{ \frac{\langle\sigma v\rangle N_\gamma}{10^{-25} \text{ cm}^3 \text{ s}^{-1}} \right\} \left\{ \frac{500 \text{ GeV}}{m_\chi} \right\}^2 \Sigma_{19} , \quad (6)$$

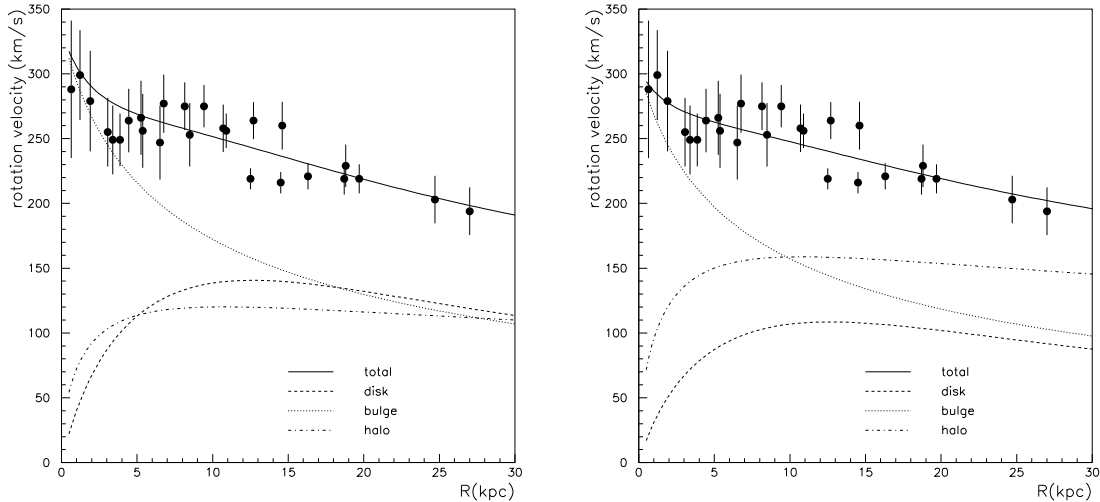


Figure 3: a  $\gamma = 1$  neutralino halo is added to the bulge and to the disk of M31. In the left panel, an intermediate case is featured with values for the mass-to-light ratios of  $\Upsilon_{bulge} = 4.2 \Upsilon_{B,\odot}$  and  $\Upsilon_{disk} = 4.2 \Upsilon_{B,\odot}$ . The right panel corresponds to a maximal halo with the same mass-to-light ratios as in Fig. 2 (see also Table 1). The global – solid – rotation curve is in good agreement with the data of [3].

where  $\Sigma_{19}$  denotes  $\Sigma$  expressed in units of  $10^{19} \text{ GeV}^2 \text{ cm}^{-5}$ .

In order to estimate the gamma-ray emission of an hypothetical neutralino halo around M31, we have considered an intermediate NFW halo with bulge and disk mass-to-light ratios of  $\Upsilon_{bulge} = 4.2 \Upsilon_{B,\odot}$  and  $\Upsilon_{disk} = 4.2 \Upsilon_{B,\odot}$  (left panel of Fig. 3). The parameter  $\Sigma_{19}$  of expression (6) reaches 1 in the inner 3.5 kpc which corresponds to 5 mrad, field of view of CELESTE and 1.2 up to 28 kpc which is the M31 radius. A fiducial model for the neutralino has been assumed with  $m_\chi = 500 \text{ GeV}$  and annihilation cross section multiplied by mean velocity and average number of  $\gamma$  in final state:  $\langle\sigma v\rangle N_\gamma = 10^{-25} \text{ cm}^3 \text{ s}^{-1}$ . The corresponding gamma-ray fluxes are respectively  $3.2 \times 10^{-13}$  and  $3.8 \times 10^{-13} \text{ photons cm}^{-2} \text{ s}^{-1}$  as presented in Table 1. In the right panel of Fig. 3, a more massive halo has been considered. The mass-to-light ratios of the bulge and of the disk are  $\Upsilon_{bulge} = 3.5 \Upsilon_{B,\odot}$  and  $\Upsilon_{disk} = 2.5 \Upsilon_{B,\odot}$ , respectively. In this more favourable situation for detection, the gamma-ray emission is increased by a factor of 3 with respect to the previous case. Recent data at radial distance  $15 \leq r \leq 30 \text{ kpc}$ , employing different data reduction analysis than that by Braun imply the presence of more mass at large radius than in Braun’s curve and a flatter mass distribution [7]. Therefore one may well be close to the most favourable case.

$\Upsilon_{bulge}$	$\Upsilon_{disk}$	$\Sigma_{19}(3.5 \text{ kpc})$	$\Sigma_{19}(28 \text{ kpc})$	$I_\gamma(3.5 \text{ kpc})$	$I_\gamma(28 \text{ kpc})$
6.5	6.4	0	0	0	0
4.2	4.2	1	1.2	$3.2 \times 10^{-13}$	$3.8 \times 10^{-13}$
3.5	2.5	3	3.7	$10.2 \times 10^{-13}$	$11.8 \times 10^{-13}$

Table 1: three different models for M31 are featured in this table. When the mass-to-light ratios of the bulge and of the disk are respectively  $\Upsilon_{bulge} = 6.5 \Upsilon_{B,\odot}$  and  $\Upsilon_{disk} = 6.4 \Upsilon_{B,\odot}$ , no halo is necessary (Fig. 1). The intermediate halo (second line) corresponds to the left panel of Fig. 3, and the massive halo (third line) to the right panel of Fig. 3. The line of sight integral  $\Sigma_{19}(R)$  is expressed in units of  $10^{19} \text{ GeV}^2 \text{ cm}^{-5}$  whereas the flux  $I_\gamma(R)$  corresponds to the number of photons collected per  $\text{cm}^2$  and per sec, for a circular region encompassing the inner 3.5 and 28 kpc, respectively. The assumed neutralino mass is  $m_\chi = 500 \text{ GeV}$  with an annihilation cross section such that  $\langle\sigma v\rangle N_\gamma = 10^{-25} \text{ cm}^3 \text{ s}^{-1}$ .

### 3 Supersymmetric model predictions

In the present section we concentrate on more specific particle physics model predictions of the  $\gamma$  - ray fluxes. The aim is to implement, test and use a computational tool which allows to scan over various observables related to supersymmetric dark matter. This is achieved through an interfacing of two public codes, DarkSUSY [9] and SUSPECT [10], which we dub hereafter DSS (DarkSUSY-SUSPECT). Significant features on both particle physics and cosmology sides are thus combined within our approach. For instance, we will study the effects of universality versus non-universality of the soft supersymmetry breaking parameters and/or the (necessary) requirement of radiative electroweak symmetry breaking, both on the cosmological relic density of the neutralino LSP as well as on the gamma-fluxes from LSP annihilation in the halo of M31 as modelled in the previous section.

#### 3.1 MSSM parameterization

We will focus mainly on the minimal supergravity scenario (mSUGRA), where the soft breaking of supersymmetry occurs in a hidden sector, which communicates with the visible sector only via gravitational interactions, and translates to the observable particle physics sector in the form of soft masses and trilinear couplings among the scalar fields as well as mass terms in the gaugino sector [8]. We make the usual simplifying assumption of common universal values of these parameters at the grand unified theory (GUT) energy



scale  $M_{GUT}$ , i.e.  $m_{scalars}(M_{GUT}) \equiv m_0, M_{gauginos}(M_{GUT}) \equiv m_{1/2}, A_{trilinear}(M_{GUT}) \equiv A_0$ . Thus, starting from the common scalar soft supersymmetry breaking (SSB) mass

$$m_{\tilde{Q}}^2 = m_{\tilde{U}}^2 = m_{\tilde{D}}^2 = m_{\tilde{L}}^2 = m_{\tilde{E}}^2 = m_{\tilde{H}_1}^2 = m_{\tilde{H}_2}^2 \equiv m_0^2,$$

the common SSB gaugino mass

$$M_1 = M_2 = M_3 \equiv m_{1/2},$$

the common SSB trilinear coupling

$$A_t = A_b = A_\tau \equiv A_0$$

and unified gauge couplings  $\alpha_1 = \alpha_2 = \alpha_3 \equiv \alpha_{GUT}$ , all taken at the GUT scale, the relevant low energy quantities are obtained from the renormalization group evolution of these parameters from  $M_{GUT}$  down to a scale of the order of the electroweak scale. At this scale electroweak symmetry breaking is required through the minimization equations [2],

$$\frac{1}{2}M_Z^2 = \frac{\bar{m}_1^2 - \tan^2(\beta)\bar{m}_2^2}{\tan^2(\beta) - 1} \quad (7)$$

$$\sin 2\beta = \frac{2B\mu}{\bar{m}_1^2 + \bar{m}_2^2} \quad (8)$$

where  $\bar{m}_i^2 \equiv m_{H_i}^2 + \mu^2 + \text{radiative corrections}$ ,  $\mu$  is the supersymmetric mixing parameter of the two higgs doublets superfields and  $B$  is the corresponding SSB parameter in the higgs potential. For a given  $\tan\beta$  at the electroweak scale (defined as the ratio of the two Higgs vacuum expectation values  $\langle H_2^0 \rangle / \langle H_1^0 \rangle$ ), one determines from the above equations the  $\mu$  parameter (up to a sign ambiguity) and the  $B$  parameter consistent with the physical value of the  $Z$  boson mass  $M_Z$ . In SUSPECT [10] the procedure is carried out including radiative corrections to the above EWSB conditions, renormalization group evolution to 1-loop order for the soft parameters, and to 2-loop order for gauge and Yukawa couplings (including threshold corrections from the supersymmetric spectrum). The full MSSM mass spectrum and couplings are computed and fed to DarkSUSY [9].

Various phenomenological constraints are taken into account (e.g. consistency with top, bottom and  $\tau$  masses, present experimental limits on superpartner and Higgs masses, limits from bottom decay  $b \rightarrow s\gamma$ , no charged LSP, ...), some of which are implemented

in SUSPECT and others in DarkSUSY<sup>2</sup>.

Apart from mSUGRA with independent parameters  $m_0, m_{1/2}, A_0, \tan \beta, \text{sign}(\mu)$ , we will also consider an alternative and less constrained case study with 7 free parameters at the electroweak scale, namely  $\mu, M_2, m_A, \tan \beta, m_{\tilde{q}}, A_b, A_t$ . Here  $M_2$  is the soft wino mass (we still assume the GUT relation between  $M_2$  and soft bino mass  $M_1$ ),  $m_A$  is the physical CP-odd higgs mass,  $m_{\tilde{q}}$  the common value of *all* soft scalar masses at the electroweak scale. Furthermore, we do not require the EWSB constraints Eq.(7,8) in this context. It should be understood, however, that such configurations are considered here only as a test case of the sensitivity of gamma fluxes and neutralino relic density to large departure from more physically motivated parameterizations such as mSUGRA. We will refer to these configurations as low energy universality (LEU).

Finally, we will also consider configurations motivated by the focus point behaviour within mSUGRA [13]. This allows in principle large  $m_0$  values (in the TeV range) without having to fine-tune the parameters in Eq.(7). This comes about due to a peculiar behaviour in the running of  $m_{H_2}^2$  from the GUT scale to the electroweak scale, which renders this soft mass fairly insensitive to the supersymmetry parameters provided that  $\tan \beta$  is moderate or large. The implication for neutralino dark matter can be important as the LSP would acquire a non negligible higgsino component (in contrast to the generic mSUGRA almost purely bino prediction). This would affect the relic density as well as the gamma fluxes from LSP annihilation into W or Z pairs, when kinematically allowed, are no more suppressed as compared to the fermion-anti-fermion channels. Nonetheless, the “naturalness” of the focus point is actually moderated by a high sensitivity to the top quark mass in relic density calculations [14]. We will thus adopt hereafter a qualitative standpoint where  $m_0$  is allowed to be in the TeV range, disregarding fine-tuning issues. We dub these configurations FP-mSUGRA.

## 3.2 Relic density

In addition to the phenomenological or theoretical constraints mentioned in the previous section, one should impose conservatively [15] that the LSP relic density be in the cosmologically favoured region  $0.1 \lesssim \Omega_\chi h^2 \lesssim 0.3$ . However, we will also consider in the region  $0.025 \lesssim \Omega_\chi h^2 \lesssim 0.1$  where we will apply a renormalization procedure on the expected fluxes.

---

<sup>2</sup>We have also deactivated the  $g_\mu - 2$  constraint. Clearly a more refined treatment should require consistency with the standard model predictions [11]. Furthermore, absence of charge and/or color breaking minima is not checked within our (exploratory) approach [12]

Over the last decade the neutralino LSP relic density has been extensively studied in the literature (for reviews cf. [16, 17, 18]). For simplicity we focus mainly on those regions of the parameter space where co-annihilation effects [19] are unimportant in the estimate of  $\Omega_\chi h^2$ . For large  $\tan\beta$  values, Higgs resonances can enhance drastically the LSP annihilation leading to very small  $\Omega_\chi h^2$ . Such effects are taken into account in our study. The actual bottom and top quark masses become a key issue in this case [20]. We come back to this point later on when discussing benchmark points.

When far from co-annihilation and resonance regions, the relic density can be estimated through [21]:

$$\Omega_\chi h^2 \simeq \frac{1.07 \times 10^9 x_f}{g_\star^{1/2} M_{pl}(GeV)(a + \frac{b}{2x_f})} \quad (9)$$

where  $x_f \equiv m_\chi/T_f \sim 25$  provides the approximate freeze-out temperature, and  $g_\star$  counts the massless degrees of freedom at the typical temperature. Here  $a$  and  $b$  are defined as usual through the Taylor expansion in relative velocity of the thermally averaged annihilation cross-section times the neutralino velocity where  $\langle \sigma v \rangle$  [22] is:

$$\langle \sigma v \rangle = a + b \frac{T}{m_\chi} + O\left(\frac{T^2}{m_\chi^2}\right) \quad (10)$$

Note that the relation (10) is no more a good approximation in cases where resonance effects on the annihilation rate become important [19].

### 3.3 mSUGRA versus general MSSM

In this section we compare the results of simulations for MSSM (DarkSUSY) with mSUGRA models (DSS).

#### 3.3.1 Benchmark points comparisons

The SUSY benchmark models have been proposed by [23, 24] to provide a common way of comparing the SUSY discovery potential of the future accelerators such as LHC or Linear Colliders. The thirteen SUSY scenarios correspond to thirteen configurations of the five mSUGRA parameters with the trilinear coupling parameter  $A_0$  set to 0. The models fulfill the conditions imposed by LEP measurements, the  $g_\mu - 2$  result (which in our case will be not fulfilled), and the relic density constraint:  $0.1 < \Omega_\chi h^2 < 0.3$ .

Table 2: benchmark models in various simulation.

model	B	C	G	I	L
$m_{1/2}$	255	408	383	358	462
$m_0$	102	93	125	188	326
$\tan\beta$	10	10	20	35	45
$\text{sign}(\mu)$	+	+	+	+	+
EWSB scale [GeV]	492.8	721.2	719.1	657.4	836.1
GUT scale [GeV]	$2.17 \times 10^{16}$	$0.30 \times 10^{16}$	$1.90 \times 10^{16}$	$1.99 \times 10^{16}$	$1.86 \times 10^{16}$
$m_{\chi^0}$	99.4	162.3	155.1	144.8	190.2
$R_g$	0.968	0.988	0.987	0.985	0.990
$\mu$	351.5	542.5	500.0	479.2	593.7
$m_A$	395.8	603.9	545.4	472.4	548.4
$M_1$	103.6	166.0	158.5	147.7	193.1
$M_2$	194.7	308.0	295.4	276.0	358.6
$M_3$	622.7	929.2	900.3	849.6	1071.
$m_{\tilde{q}}$	537.8	787.0	767.2	718.7	907.9

The aim of the present section is to derive the gamma ray fluxes for some of these benchmark models with our current MC simulation programs: DarkSUSY [9] and SUSPECT [10], which were described previously. The value of  $\Omega_\chi h^2$  is calculated in the DarkSUSY part where only  $\chi^+ \chi_2^0$  co-annihilations and annihilations related to the Higgs sector channels are included. As a consequence of these software limitations, the physically accessible SUSY domain in this study corresponds to models B,C,G,I and L of [23, 24]. The simultaneous use of the SUSPECT and DarkSUSY package allows to perform RGE evolution from the GUT scale to EWSB scale. Table 2 presents the initial GUT scale parameter values as well as other input parameters to DarkSUSY, calculated by SUSPECT ( $\mu$ ,  $M_1$ ,  $M_2$ ,  $M_3$ ,  $m_{\tilde{q}}$ ,  $m_A$ ). The GUT scale and EWSB scale values are also quoted as well as neutralino mass and gaugino fraction,  $R_g$ .

Table 3 presents the resulting relic density values with different theoretical assumptions corresponding either to mSUGRA or to LEU as described in section 3.1 whereas Table 4 gives results for  $\gamma$ -ray flux,  $\Phi_\gamma$  respectively. In order to be free from the Galactic Centre halo modelling, a renormalisation factor on the astrophysical part of the  $\gamma$  flux computation has been applied. This allows a meaningful comparison between our results and those of [23, 24]. In case of comparison between mSUGRA and LEU, one has to choose some common features of the two configurations. We do this by choosing for the

Table 3: the relic neutralino density, i.e.  $\Omega_\chi h^2$ , as obtained in our simulations assuming a bottom mass of  $m_b = 4.61 \text{ GeV}$  and neglecting radiative corrections.

model	B	C	G	I	L
DarkSUSY	1.37	4.20	1.34	0.26	0.11
DSS	0.19	0.32	0.29	0.18	0.10
paper [39]	0.18	0.14	0.16	0.16	0.21

Table 4: the predicted  $\gamma$ -ray flux in units of  $10^{-12} \text{ cm}^{-2} \text{ s}^{-1}$  from the galactic center for  $\gamma$ -rays with energy  $E_\gamma > 1 \text{ GeV}$  emanating from M31 within a solid angle  $\Theta = 10^{-3} \text{ sr}$ .

model	B	C	G	I	L
G.C. NFW DarkSUSY	293.5	29.8	207.1	1447.0	2450.0
G.C. NFW DSS	293.0	30.9	209.1	1442.0	2458.2
paper [39]	84.29	10.19	63.90	535.0	992.4
paper [39] renormalized	204.8	24.76	155.3	1300	2412
M31 NFW DSS	3.5	0.37	2.5	17.3	30.0

low energy universal masses in the LEU case, some of the representative values for the soft masses (and the  $\mu$  parameter) at the electroweak scale, as given by the mSUGRA analysis. In the case of the soft scalar masses the choice is not unique. The numbers given in Tables 3 and 4 illustrate typical sensitivities.

As far as benchmark points with large  $\tan\beta$  are concerned, the relic density is very sensitive to the input bottom mass since the latter controls the position of the s-channel CP-odd Higgs exchange pole [20].

The effect of applying radiative corrections has been found to be below 25% on flux predictions. The results obtained here are also compared to those in [23], where a different mSUGRA MC has been used and a more complete set of co-annihilation channels has been included. The observed differences on flux predictions of at most  $\sim 25\%$  between our results and those in [23] may well be explained by different treatments of the fragmentation processes with  $\pi^0$  in the final state.

The results given in Table 4 on the  $\gamma$ -ray flux from the Galactic Center are given for NFW [5] halo density parameterization, determined above a threshold of 1 GeV within a solid angle of  $10^{-3} \text{ sr}$ . For comparison, the flux from M31 has been also evaluated for the same

energy threshold and acceptance value, assuming a NFW profile and model 3 in Table 1.

### 3.3.2 Predictions from “wild scan” simulations

We have also performed a “wild scan” by having less restrictive conditions on the supersymmetric parameters (referred to as “LEU” - see above). To achieve this, three thousand models have been simulated in the  $0.025 \lesssim \Omega_\chi h^2 \lesssim 0.3$  region. The value of the lower limit on  $\Omega_\chi h^2$  equal to 0.025 has been used with a renormalization procedure for flux estimation described below (for  $\Omega_\chi h^2 \lesssim 0.1$ ). The low values of  $\Omega_\chi h^2$  may indicate that the main component of the dark matter is not the SUSY LSP and other contributions should be considered. The conditions of the performed simulations were for:

LEU 7 parameters:

$$10. < |\mu| < 5000.$$

$$10. < |M_2| < 1600.$$

$$10. < m_A < 1000.$$

$$1.001 < \tan(\beta) < 60.$$

$$50. < m_{\tilde{q}} < 1000.$$

$$-3. < A_t/m_{\tilde{q}} < 3.$$

$$-3. < A_b/m_{\tilde{q}} < 3.$$

mSUGRA 5 parameters:

$\text{sign}(\mu)$  not constraint

$$50. < m_0 < 3000.$$

$$50. < m_{1/2} < 1600.$$

$$0.1 < |A_0| < 2000.$$

$$3. < \tan(\beta) < 60.$$

Only co-annihilation with  $\chi^+$  or  $\chi_2^0$  has been considered which is relevant when the higgsino component of neutralino becomes substantial. All results for the integrated gamma fluxes from M31 as a function of the  $\chi_1^0$  mass were obtained for a NFW profile and model 3 in Table 1, and for  $\gamma$ -ray energy threshold of 30 GeV. The decay channels with  $\pi^0$  in the final state subsequently decaying into  $\gamma$ s, such as  $b\bar{b}$ ,  $W^+W^-$ ,  $Z^0Z^0$ ,  $HH$ , ..., were provided by the PYTHIA 6.1 program which is included in data format of the DarkSUSY package.

Figure 4 shows the integrated flux as a function of the neutralino relic density  $\Omega_\chi h^2$ . The shape of the envelope corresponding to maximal fluxes can be understood qualitatively

by using Eq. (2), Eq. (9), and Eq.(10) and maximizing  $\langle \sigma v \rangle$  in the parameter space. For instance in the  $b\bar{b}$  channel,  $\langle \sigma v \rangle$  reaches a maximum when the lightest sbottom is degenerate with the LSP leading to  $\langle \sigma v \rangle_{max} \propto m_\chi^{-2}$ , that is  $\Omega_\chi^{min} \propto m_\chi^2$ . Combining this with the appropriate dependence of  $N_\gamma$  on  $m_\chi$  which can be obtained from the energy distribution [25]

$$\frac{dN_\gamma}{dE} = a \frac{e^{-b\frac{E}{m_\chi}}}{m_\chi (\frac{E}{m_\chi})^{1.5}} \quad (11)$$

by integrating over the full spectrum,

$$\int_{E_{min}}^{\infty} \frac{dN_\gamma}{dE} dE = 2a \left\{ \sqrt{\frac{m_\chi}{E_{min}}} e^{-b\frac{E_{min}}{m_\chi}} + (Erf[\sqrt{\frac{bE_{min}}{m_\chi}}] - 1) \sqrt{b\pi} \right\} \quad (12)$$

where  $E_{min}$  is an acceptance energy cut, one recovers a behaviour similar to the envelope shown in Fig 4.

A renormalisation procedure has been used for low  $\Omega_\chi h^2$  values where the dark matter halo should not be dominated by the neutralinos. For values of  $\Omega_\chi h^2$  below 0.1 the predicted flux is renormalized by the ratio  $(\Omega_\chi h^2 / 0.1)^2$  to account for neutralinos only contributing partially to the dark halo. As a result of this procedure, the obtained fluxes went down by a factor of 10 at low values of  $\Omega_\chi h^2$ . The effect of the renormalization procedure described above is also shown in Fig. 4.

Figure 5 presents the integrated gamma flux as a function of  $m_\chi$  for the LEU scheme. The expected fluxes for M31 are of the order of  $10^{-13} \text{ } \gamma \text{ cm}^{-2} \text{ s}^{-1}$  and show only a weak dependence on the gaugino fraction of the neutralino. Comparing to mSUGRA predictions shown in Fig. 6, clear differences are observed:

- the unification at GUT scale and electroweak symmetry breaking constraints lead to the exclusion of an important number of models in mSUGRA models, which are present in the LEU scheme,
- the mSUGRA model reduces the number of viable Higgsino like models when compared to the LEU model, and
- mSUGRA models generally show factor  $\sim 5$  lower fluxes at low values of  $m_\chi$  as compared to LEU models.

The benchmark model points are also presented.

Figure 7 presents mSUGRA results in case of the so-called ‘‘Focus Point’’ inspired scenario where  $m_0$  values may vary up to 3 TeV. In this case there are more viable models with a neutralino of comparatively large Higgsino content than in mSUGRA and the mean fluxes

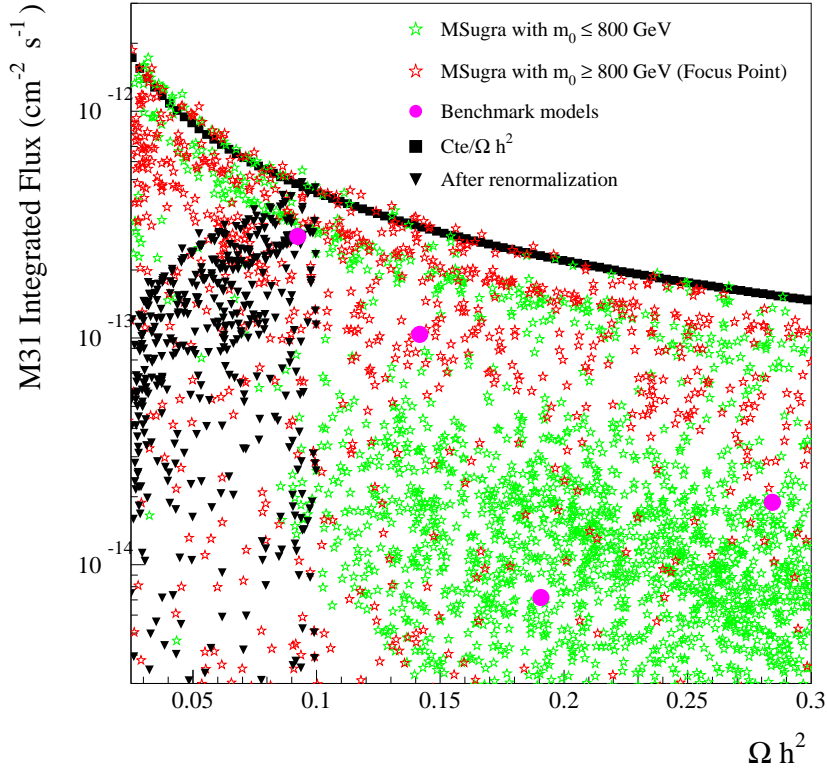


Figure 4: the integrated  $\gamma$  flux from M31 as a function of  $\Omega_\chi h^2$ . A renormalization procedure for  $\Omega_\chi h^2 \leq 0.1$  has been applied on flux values as described in the text.

reach values predicted by LEU.

The CP-odd Higgs mass resonance effect (i.e.  $m_A \approx 2m_{\chi^0}$ ) on the annihilation cross section and predicted fluxes has also been examined. Figure 8 presents an increase of the integrated flux at the  $m_A$  pole by at least an order of magnitude compared to the region far from the resonance. This effect reflects increase of the predicted fluxes for large  $\tan\beta$  shown in Fig. 9, as the CP-odd Higgs s-channel dominates at large  $\tan\beta$  in the mSUGRA frame.



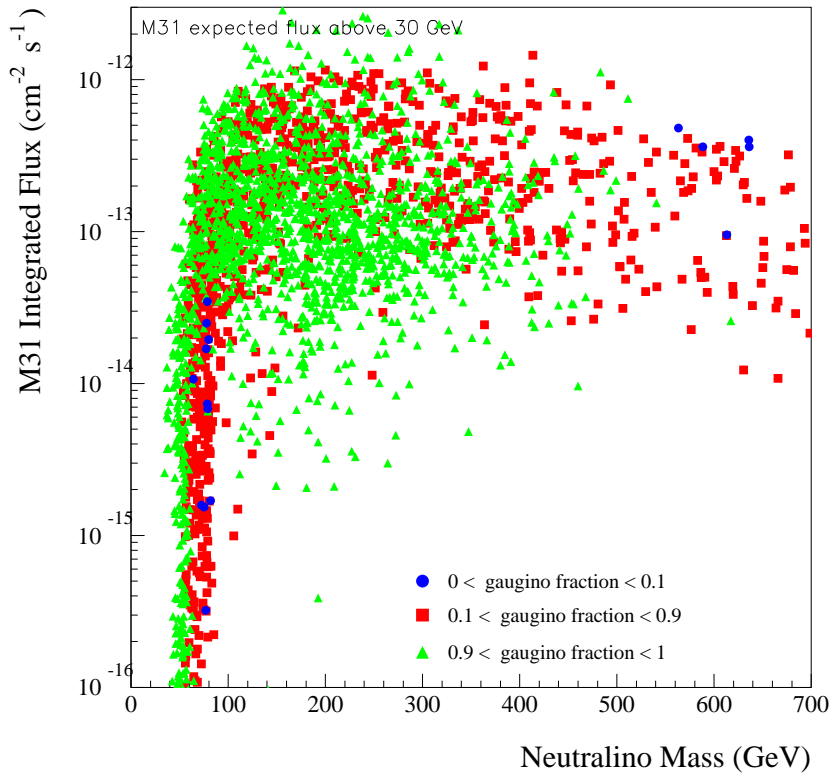


Figure 5: the integrated  $\gamma$  flux from M31 as a function of  $m_\chi$  for  $E_\gamma > 30\text{GeV}$ . Each point corresponds to a model in our "wild scan" LEU simulations. Three different ranges of gaugino fraction are considered.

## 4 Detection of Dark Matter in M31 with CELESTE

### 4.1 The CELESTE experiment

The "Cherenkov Low Energy Sampling and Timing Experiment" (CELESTE) is located on the site of Thémis in the French Pyrénées. It detects  $\gamma$ -rays in the high energy domain and was designed to fill the energy gap between satellites and imaging atmospheric Cherenkov telescopes (IACTs). While the former have been so far limited to  $\sim 10$  GeV because of a too small effective detection area, the energy domain covered by the latter starts at  $\sim 200$  GeV due to the noise arising from the night sky background. The energy window around 50 GeV has been opened by CELESTE during the winter 1999-2000 by

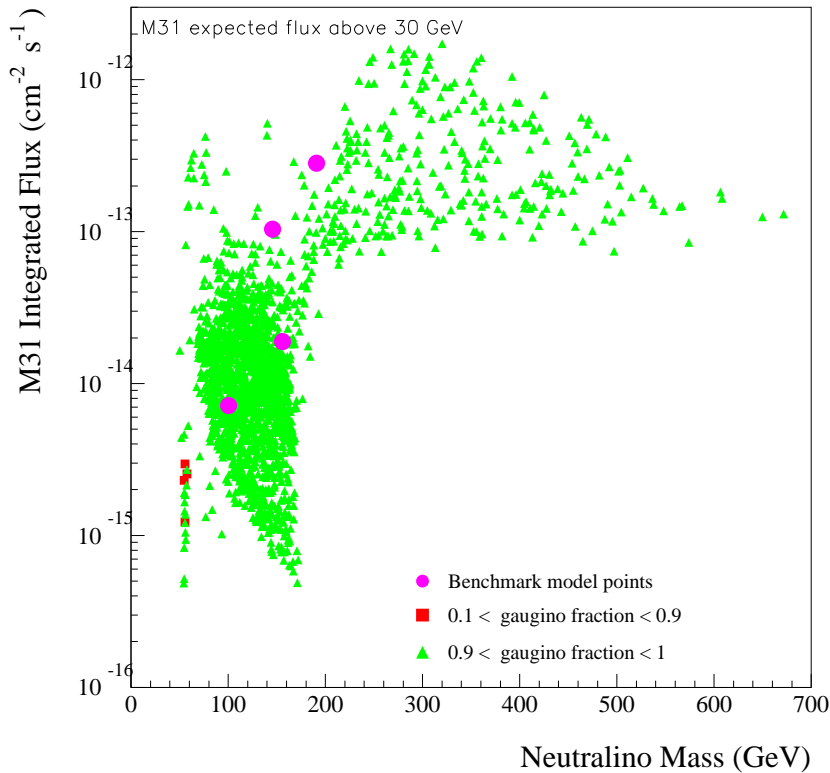


Figure 6: the integrated  $\gamma$  flux from M31 as a function of  $m_\chi$  in mSUGRA scheme. The constraints applied (as described in the text) remove large number of LEU allowed configurations.

the detection of the Crab nebula and its flux measurement at 60 GeV [26]. Nearly at the same time, CELESTE detected the Active Galactic Nuclei (AGN) Mkn 421 during a series of flares. It was the first sub-100 GeV detection of this nearby blazar and the emission observed by CELESTE showed a clear correlation with the flux recorded above 250 GeV by the CAT telescope, operating on the same site [27]. Before these results, the sub-100 GeV region was the only part of the electromagnetic spectrum which remained unexplored. The access to this region is of great importance for a number of key questions in high-energy gamma-ray astrophysics. For instance, the high-energy part of some AGNs can dominate the entire spectrum, giving new insight into their structure as well as the particle acceleration and cooling processes occurring in their vicinity. Pulsars could be also very promising sources : since their  $\gamma$ -ray spectrum is believed to decrease sharply at a few tens of GeV, the observation of the predicted spectral cutoff should strongly constrain the models describing the particle acceleration in their magnetosphere. Concerning galac-

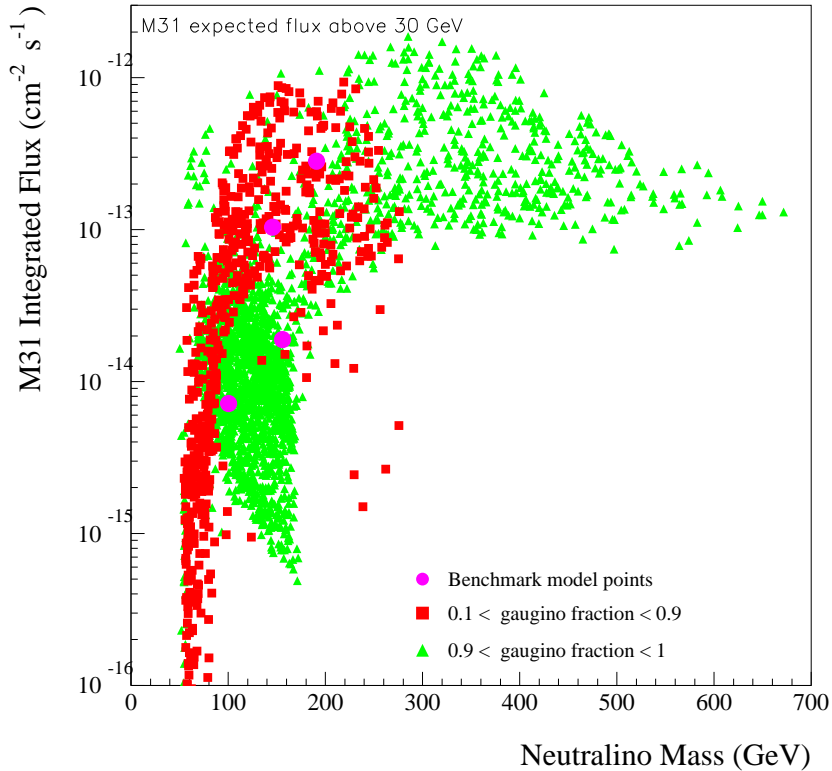


Figure 7: the integrated  $\gamma$  flux from M31 as a function of  $m_\chi$  in the so-called Focus Point scenario (large  $m_0$  values).

tic cosmic-rays, the current belief of their acceleration in shell-like supernovæ remnants could be also tested in a few cases by the observation of high-energy  $\gamma$ -rays. Apart from astrophysical issues, we propose here to use CELESTE for the study of dark matter and searches for the indirect signatures of neutralinos, namely their gamma-ray signal above 50 GeV coming from neutralino annihilations in M31. At the latitude of Thémis (42° North), M31 transits very close to Zenith.

The CELESTE experimental setup is fully described in [26]. This detector records the Cherenkov light emitted by the secondary particles produced during the development of the cosmic-ray atmospheric showers. In order to reduce the night-sky noise and to achieve a low energy threshold, CELESTE uses 40 heliostats (53 since January 2002) of the former solar plant in Thémis, with a total collection area of  $\sim 2000\text{m}^2$ . An efficient discrimination between  $\gamma$  and hadron-induced showers allows to extract the  $\gamma$ -ray signal from the more

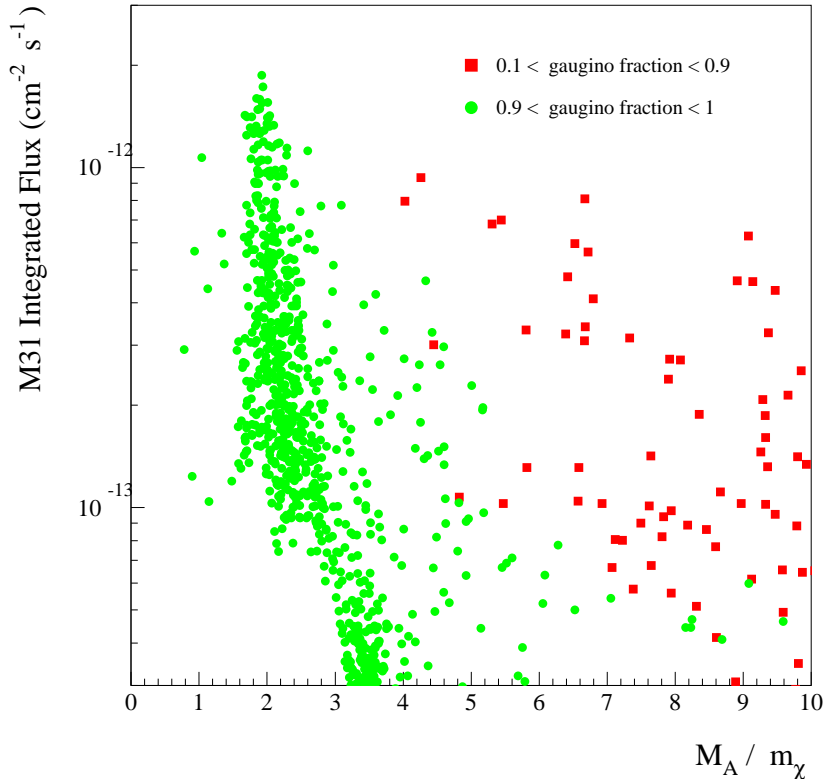


Figure 8: the integrated  $\gamma$  flux from M31 as a function of  $M_A/m_\chi$ . Here only fluxes above  $10^{-14}$  are presented. A large enhancement at  $2m_\chi$  equal to  $M_A$  is observed.

abundant charged cosmic-ray background (mostly protons, helium nuclei and electrons). The event analysis is based on the differences between both types of showers regarding the homogeneity and the time dispersion of the Cherenkov light pool as sampled by the heliostats. After the detector trigger and all analysis cuts, the  $\gamma$ -ray acceptance at Zenith has been parameterized as a function of the energy [28] :

$$\mathcal{A}(E) = A_0 \left[ 1 - \exp \left( - \frac{E - E_0}{E_c} \right) \right], \quad (13)$$

with  $A_0 = 1.37 \times 10^4 \text{ m}^2$ ,  $E_0 = 34.7 \text{ GeV}$  and  $E_c = 56.2 \text{ GeV}$ .

## 4.2 Simulation results

The flux predictions of mSUGRA models were folded with the acceptance function of the CELESTE detector. Figure 10 shows the expected count rates from M31 in units of

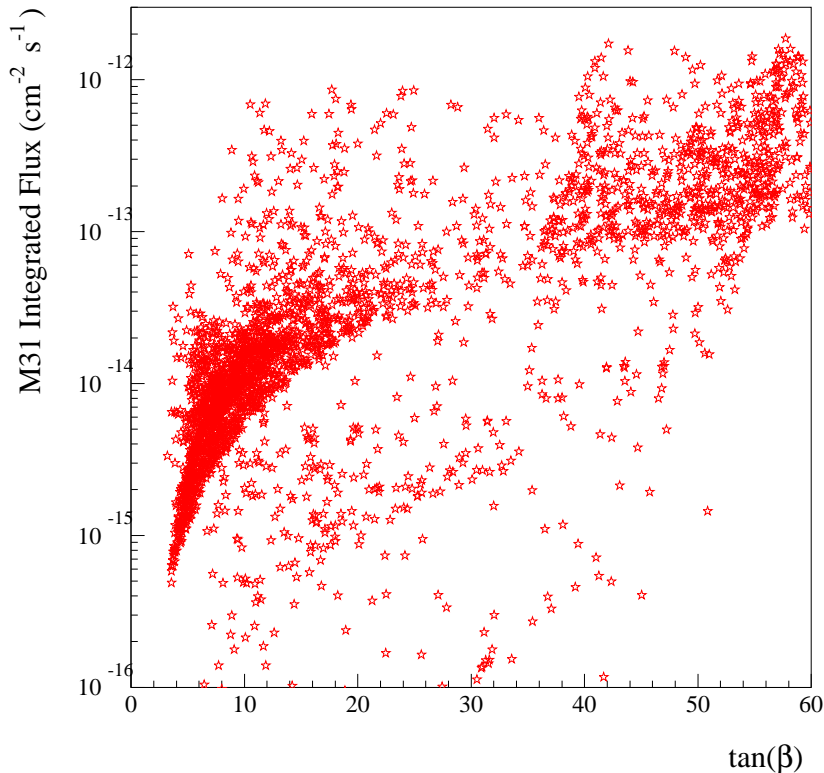


Figure 9: the integrated  $\gamma$  flux from M31 as a function of  $\tan\beta$ . Here the highest fluxes also correspond to the CP-odd Higgs contributions.

$\gamma/\text{min}$ . The most optimistic models predicts values of the order of  $10^{-3}$ , which should be compared with the  $4.9 \gamma/\text{min}$  which are observed by CELESTE from the Crab nebula (the standard candle for high-energy  $\gamma$ -ray astronomy) [28]. Note that these results were obtained without any signal enhancement effect expected from clumpiness of the dark matter halo or possible black hole neutralino accretion. Since the sensitivity level of atmospheric Cherenkov detectors is proportional to  $1/\sqrt{T_{\text{obs}}}$ , only sources with a flux of a few tenths of the Crab nebula flux can be detected within realistic observation times. Therefore the overall enhancement due to astrophysical effects has to exceed at least a factor of 100 for detection of a  $\gamma$ -ray signal from neutralino annihilations to become feasible. The impact of such effects will be addressed in the next section.

A possibility of the shape discrimination with the energy differential flux measurement in CELESTE has been also studied. The expected shape for  $\gamma$ -rays produced in  $\chi^0\chi^0$  anni-

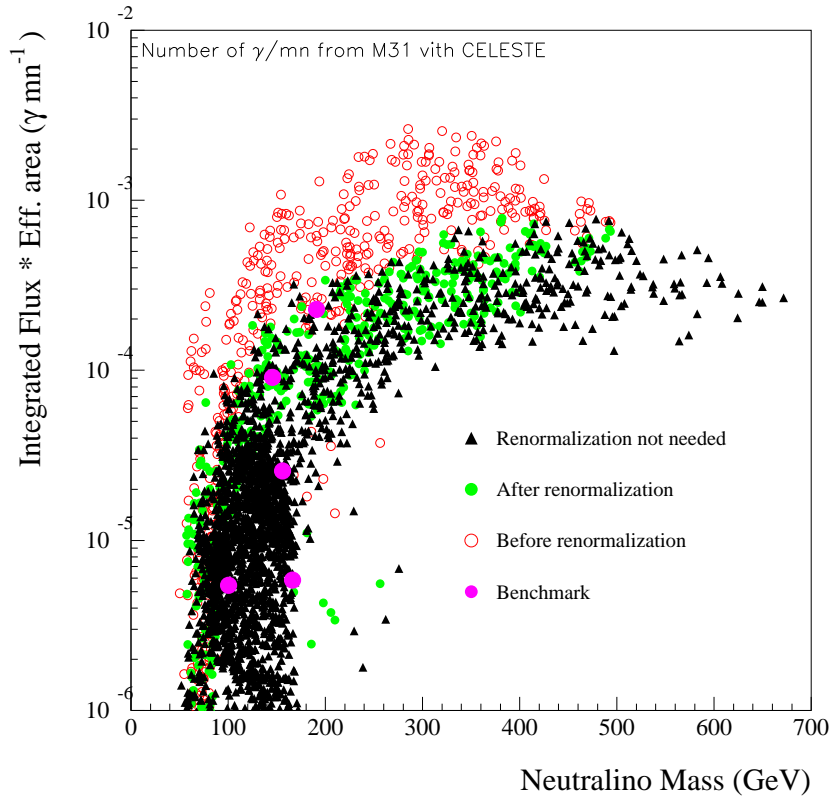


Figure 10: number of  $\gamma/min$  as expected from M31 with CELESTE acceptance in mSUGRA models.

hulations are described by a decreasing exponential function with the exponent strongly depending on  $m_\chi$ . This sharp exponential cut-off should be compared with standard astrophysical source power law expectations.

The shape discrimination relies on the assumption of the  $\gamma$  detection from the considered source, in our case M31. The event selection and cuts on the kinematical variables of the  $\gamma$  candidates allow to enhance the  $\gamma$  contribution to the measured sample with respect to the charged cosmic-ray initiated showers. In order to reduce further the charged cosmic-ray background and to optimize the signal to background ratio, various procedures such as a sliding window type method can be considered. This analysis will be addressed in details elsewhere.

Figure 11 presents predicted energy differential distributions for various  $m_\chi$  ranges after the renormalization of the total integrated fluxes. Here an almost scaling variable equal to  $E_\gamma/m_\chi$  was used as proposed by [25]. No background contribution has been taken into

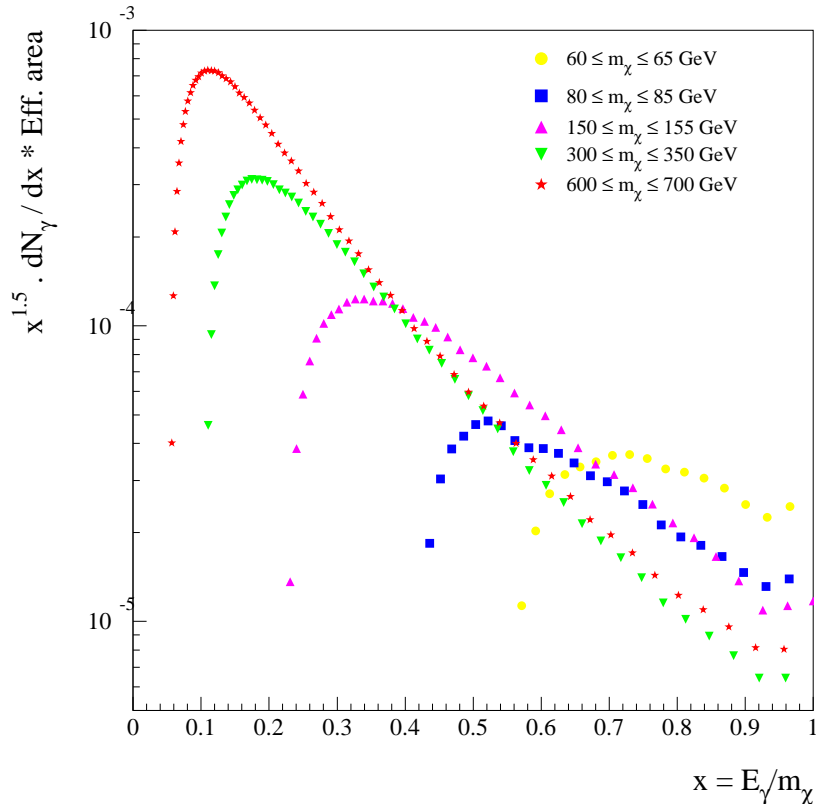


Figure 11: a shape variation of the scaling variable  $x$  equal to  $E_\gamma/m_\chi$  [25] for various  $m_\chi$  values. A weak dependence on  $m_\chi$  comes from different annihilation channels.

account here. These results suggest an increase in sensitivity with  $m_\chi$ . However, due to the CELESTE acceptance varying with energy, a realistic discrimination measurements can only be considered for neutralino masses above 200 GeV. It is interesting to note that only models with substantial co-annihilation and large  $\tan\beta$  can lead to acceptable dark matter densities for  $\Omega_\chi h^2$  above 200 GeV.

## 5 Impact of Astrophysical parameters

### 5.1 Halo Clumpiness

Early simulations of the growth of CDM halos found smooth tri-axial structures, but higher resolution simulations revealed that a significant fraction of the mass may lie in substructures (sub-halos) orbiting in virialized dark matter halos [29, 30, 31]. Such

substructures seem to extend down to the smallest mass scale, possibly well below that of the most massive globular clusters.

The CDM scenario, however, predicts a larger number of substructures in galactic halos than the observed number of dwarf satellites in the Milky Way [30, 32]. The cases of gas expulsion by supernova-driven winds or the failure of gathering enough gas for stellar formation were considered in [30] as possible explanations. In this case there would be a large number of clumps with few stars, and some of the known high-velocity gas clouds may possibly trace them. It has been also shown recently that there is good agreement between the rotation curves of the largest satellites and those found in N-body simulations, provided star formation is less efficient in these satellites [33]. The possibility that the anomalous image flux ratios observed in several gravitational lenses could be explained by low mass satellites in the lensing galaxy was also explored [34]. It was found that the required projected satellite mass fraction is of the same order as those predicted in CDM simulations, illustrating that there is general agreement between the underlying theory for structure formation and observed structures.

In order to estimate the effect of clumpiness we calculate first the contribution to the flux of a DRACO-type object with virial velocity  $v = 10 \text{ km s}^{-1}$ , and central mass  $M \approx 10^8 M_\odot$  modeled by using a NFW profile with scale radius  $r_s = 0.4 \text{ kpc}$  and density  $\rho_0 = 6 \times 10^{-24} \text{ g cm}^{-3}$ . This is obtained by calculating the sum of the line of sight integral  $\Sigma$ , as defined in Sect. 2, over the field of view of CELESTE which we denote by  $\Sigma^{10}$  ( $\Sigma^{10} = \Sigma^{19}(3.5 \text{ kpc})$  defined in section 2). It is expressed in units of  $\equiv 10^{19} \text{ GeV}^2 \text{ cm}^{-5}$  as before. Such a single DRACO-type clump orbiting around M31 would yield  $\Sigma_D^{10} \approx 0.03$ , to be compared with  $\Sigma_{M31}^{10} \approx 3$  for M31 (cf. Sec. 2).

Now we consider the mass and the radial distribution of clumps orbiting around a halo.

The sub-halo mass function is a power law close to  $dn(m)/dm \propto (m/M_H)^{-1.9}$  [29] where  $M_H$  is the mass of the halo. The radial distribution of clumps in a halo, deduced from N-body simulations, behaves as  $n(r) \propto [1 + (r/r_c)^2]^{-3/2}$  [35]. Combining these two equations we obtain the distribution of clumps having a mass  $m$  at radial distance  $r$ :

$$n(r, m) \propto (m/M_H)^{-1.9} [1 + (r/r_c)^2]^{-3/2} \propto v^{-3.8} [1 + (r/r_c)^2]^{-3/2} \quad (14)$$

where  $v$  is the virial velocity of the clump. This equation is normalized to the number of clumps of a given mass predicted by CDM simulations.

About 1000 clumps with velocities above  $v = 10 \text{ km s}^{-1}$  are expected in a galactic halo having the mass of M31 [6]. We truncate the clump mass distribution between  $1 \leq v \leq 10 \text{ km s}^{-1}$ . We consider two spatial distributions of clumps: a compact distribution with



core radius  $r_c \sim 16$  kpc and a more extended distribution with  $r_c \sim 30$  kpc. Both are independent of the clump mass. In these profiles, around 75% of the clumps are within the core radius.

The total integrated contribution of clumps with  $v \geq 1$   $\text{kms}^{-1}$  is  $\Sigma \approx 2500 \times \Sigma_D = 77$ . Therefore the flux from M31 may be boosted by a clumpiness factor  $\sim 77/3 \approx 25$ . The clumps in the field of view of CELESTE yield respectively  $\Sigma^{10} = 20$  for  $r_c \sim 16$  kpc and  $\Sigma^{10} = 10$  for  $r_c \sim 30$  kpc, that is a factor 3.3 – 6.6 larger than the smooth profile of M31.

Globular clusters are known to continuously loose stars due to tidal forces from the halo gravitational potential. Mass is stripped from the outer regions of globular clusters and evaporates mainly at each passage through the disk. This is why it is generally argued that globular clusters do not have dark matter except perhaps in an inner bubble. The structural evolution of sub-halos was recently analyzed in [36], which shows that the tidal radius of distant satellites is well beyond their optical radius. This may also explain why the distant globular cluster Palomar 13 (at a distance of 24.3 kpc) is well fitted by a NFW profile [37], i.e. this anomalous globular cluster could, in fact, be a Milky Way dark clump which has not been destroyed or modified by the galactic tidal field [38]. The central mass-to-light ratio of the distant satellites Palomar 13 and DRACO (at a distance of 80 kpc) are, respectively, 40  $(M/L)_\odot$  and 80  $(M/L)_\odot$ , whereas for nearby globular clusters it is approximately 3  $(M/L)_\odot$ . We assume that this is the signature of enhanced particle evaporation in the inner region of clumps. To account empirically for this effect we have divided by 2 the central density of the clumps at radial distance  $r = 20$  kpc, by 20 that of objects at  $r = 10$  kpc and have ignored clumps at smaller radius. With this hypothesis the most massive objects within  $r = 10$  kpc have a mass  $< 5 \times 10^6 M_\odot$ . In any case, a significant fraction of more massive objects is forbidden by the observations because it would dynamically heat the disk (see below).

With the hypothesis of evaporation, the integrated contribution of clumps is  $\Sigma = 11 - 34$  for the whole of M31 and to  $\Sigma^{10} = 0.75 - 2.2$  in CELESTE's field of view, indicating only very modest enhancement factors of the  $\gamma$ -ray signal.

If a large number of massive satellites orbit within the M31 halo, their passages through the disk causes disk heating [39] or may induce warping motions [40]. This is confirmed by recent N-body CDM simulations of the Milky Way [41]. In the case of a  $\Lambda$ CDM cosmology, however, the clumps are less massive and are located at larger radial distance than in standard CDM, so only a small number get near the disk. In that case they do not heat the disk efficiently [42, 41]. We have already approximately accounted for the first effect by ignoring the most massive clumps with mass  $10^9 M_\odot$  in the inner regions

of galaxy. In order to account for an “extended halo distribution”, as in [41], we have considered the same clump distribution as before but with core radius 100 kpc and the same mass spectrum. With that distribution the clump flux in CELESTE’s field of view is  $\Sigma^{10} = 2.2$  without evaporation, or  $\Sigma^{10} = 1.0$  with the hypothesis of evaporation.

These  $\gamma$  ray signal enhancement factors due to halo clumpiness should be compared to those determined by N-body simulations of Milky Way type objects. Whereas earlier results by one group [43] indicate a two order of magnitude effect, more recent simulations [44] find only a factor  $\sim 2$  enhancement. Another study performed on the clumpiness enhancement factor, in particular in case of M87, observation [45] predict values between 13 and 40. These calculations were extended for Milky Way or M31 type galaxy case leading to the values of the clumpiness enhancement factor of the order of 20 [46].

## 5.2 Black hole accretion

The central region of M31 contains a very compact object with a mass  $\sim 3.6 \times 10^7 M_{\odot}$  which is assumed to be a supermassive black hole (SBH) [47, 48]. The dynamical effect of a SBH on a distribution of nearby WIMPS was studied by [48] in the case of the Milky Way. The adiabatic growth of a SBH at the center of a halo produces a spike with density  $\rho \propto r^{-\gamma}$ ,  $2.2 \leq \gamma \leq 2.5$  within a radius  $\sim 10$  pc for a SBH like that in M31. In such a spike the density reaches the annihilation density  $10^8 M_{\odot} \text{ pc}^{-3}$  in a significant region surrounding the black hole producing a huge enhancement of the annihilation flux. This calculation assumes a very high accretion rate and a stable dynamical regime during an extremely long period. In fact the accretion rate for the assumed black hole adiabatic growth is much higher than the current estimates of present-day growth-rates [7, 49]. Several authors have discussed more realistic scenarios (i.e. [50, 51]). In the CDM scenario, large halos grow through the merging of smaller building blocks. Galaxies as massive as the Milky Way or M31 have certainly experienced significant merging in the last Gyrs. There may be several SBH progenitors coming from the mergers, a SBH may be spiraling into the galactic potential. Motions of the SBH transfer energy to the particles lowering their density [52]. Thus, even if at early times a massive BH was present in a dense environment resulting in a rapid adiabatic growth of the BH surrounded by a dense spike, there are a number of accidental events and perturbations during the life of the SBH which all tend to destroy the spike. Nevertheless a SBH will continuously accrete material. If it is coinciding with the dynamic center of a galaxy for a sufficiently long period it will built a central dark matter density cusp.

We performed N-body simulations assuming initial dark matter density profiles of  $\rho \propto$

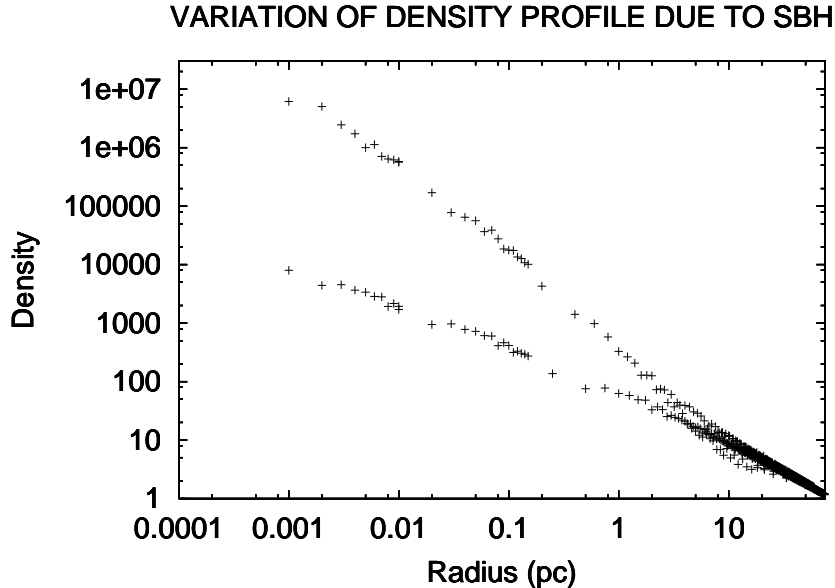


Figure 12: example of simulation showing the variation of density profile due to a massive SBH of  $3.7 \times 10^7 M_{\odot}$ . The initial profile is in  $\rho \propto r^{-0.75}$ . The final profile in  $\rho \propto r^{-1.5}$  is reached in less than  $10^6$  yrs. The density is in  $M_{\odot} \text{ pc}^{-3}$ .

$r^{-\alpha}(1 + r/r_c)^{-\beta}$  with  $0 \leq \alpha \leq 1$  and under the hypothesis of the existence of a massive central black hole - SBH. These simulations were performed with the aid of the public code Gadget [53]. In each case, the density distribution reaches a stable limit with  $\rho \propto r^{-1.5}$ , independent of the initial profile, within dynamical time of  $10^6$  yrs. An example of such simulations is shown in Fig. 12. This illustrates that a stable configuration which may be build in within a relatively short time.

The  $\gamma$ -ray flux enhancement due to the existence of such a dark matter spike as compared to a NFW profile is of the order of  $1 + [\ln(r_{max}/r_{min}) - 1] r_{max}/R$  where  $r_{min}$  and  $r_{max}$  are respectively the minimum and maximum radius of the profile in  $r^{-1.5}$  and  $R$  is the radius of the initial region with profile in  $r^{-1}$ . Taking  $R = 3.5$  kpc,  $20 \leq r_{max} \leq 100$  pc, and  $r_{min} = 10^{-5}$  pc which is  $\sim 11$  Schwarzschild radii, we get an only modest enhancement factor between 1.08 and 1.45. It is seen that the enhancement factor is small, nevertheless, the presence of the SBH in this complicated multicomponent object warrants a singular profile at small radius. This is also important with regard to evidence that the universal singular CDM profiles [54, 55] are not seen in the dark halos of low surface brightness galaxies [56]. In these objects, however, there are numerous suggestions for a hidden baryonic component [57, 58, 59] which may modify its inner profile complicating the

Clump distribution	Dynamics	SBH environment	$\Sigma$	$\Sigma^{10}$
compact	no evaporation	SIS spike	165	100
extended	no evaporation	SIS spike	140	90
compact	no evaporation	$\rho \propto r^{-1.5}$	80	20
extended	no evaporation	$\rho \propto r^{-1.5}$	55	6
compact	evaporation	$\rho \propto r^{-1.5}$	25	6
extended	evaporation	$\rho \propto r^{-1.5}$	40	5

Table 5: impact of astrophysical parameters such as clumpiness of the M31 halo and SBH in its centre, on flux predictions, smooth and clump contributions added.

interpretation of dwarf halos [60].

Finally in some cases the hypothesis of a central spike may be valid. This may happen if there is a density increase during a short period near the SBH, for example when a massive clump is falling in the SBH. As soon as the profile is steeper than  $r^{-1.5}$  the logarithmic term in the enhancement factor is replaced by a power of the inner radius. In the case of a singular isothermal (SIS) spike of 1 pc the total flux within 3500 pc is boosted by a factor 29. The impact of clumpiness and black holes are summarized in Tab. 5.2. The global enhancement factor on expected flux may vary between 5 and 100, depending on the clumpiness of the halo and CDM-accreting SBH. In particular, the large variation between  $\Sigma$  and  $\Sigma^{10}$  in case of an extended clump distribution (last line of Table 5) is due to the small angular size of the instrument compared to the compact distribution case (line 3 of Table 5).

## Conclusions

The putative dark matter content of M31 has been estimated and modelled from its observed rotation velocity profile, by adding a NFW dark halo to the observed disk and bulge component.

The study of the benchmark models in case of M31 allowed to qualify the DarkSUSY and SUSPECT MC programs used for gamma flux predictions in CELESTE experiment. Only models I and L (large  $\tan\beta$ ) could be considered as favourable for the detection. This conclusion is confirmed by a further study of the so-called “wild scan” simulation in mSUGRA scheme. Various aspects such as dependence of the results on heavy quark masses or CP-odd higgs pole contribution have been investigated.

We have taken into account the atmospheric electron and CR proton backgrounds to the M31 signal and applied the CELESTE gamma-ray energy dependent acceptance factors. Assuming a smooth neutralino halo around M31 leads to photon rates at the telescope of order a few  $10^{-3}$  counts per minute. The strongest signal corresponds to supersymmetric configurations where the neutralino mass  $m_\chi$  exceeds  $\sim 200$  GeV. As a realistic observation would require at least a signal of order a tenth of that of the CRAB – 4.9 photons per minute – we estimate that a gamma-ray annihilation signal from M31 is beyond the reach of an atmospheric Cerenkov detector of the CELESTE generation if the neutralinos are smoothly distributed in that galaxy. On the other hand, if the halo is made of clumps with inner profiles à la Moore or if there is strong accretion going on around the central black hole, the expected signal may be enhanced by two orders of magnitude and could become detectable. We conclude therefore that a survey of M31 with CELESTE is worth being undertaken.

## Acknowledgements

We would like to thank Jean-Loic Kneur for his help in running the SUSPECT program and building the interface between SUSPECT and DarkSUSY. We are also very much indebted to Piero Ullio for the time he spent on useful discussions about the DarkSUSY program and the physics related to the studied subjects. We thank the French GDR “PCHE” groups for supporting this study.

## References

- [1] J. R. Primack, 2001, astro-ph/0112255 To appear in Proceedings of International School of Space Science 2001, ed. Aldo Morselli (Frascati Physics Series).
- [2] H.P. Nilles Phys. Rep. 110 (1984) 1; H.E. Haber, G. Kane, Phys. Rep. 117 (1985) 75; R. Arnowitt, P. Nath, Report CTP-TAMU-52-93; M. Drees, S.P. Martin, hep-ph/9504324;”
- [3] R. Braun, 1991, ApJ 372, 54.
- [4] B. Guiderdoni, & Rocca-Volmerange, B. 1987, A & A 186. 1.
- [5] J.F. Navarro, C.S. Frenk and S.D.M. White, Astrophys. J. 462 (1996) 563-575.
- [6] B. Moore et al., Phys. Rev. D 64 (2001) 063508.
- [7] A. Klypin, H. Zhao, R.S. Somerville, 2001, astro-ph/0110390.
- [8] R. Barbieri, S. Ferrara, C. A. Savoy, Phys. Lett. B 119 (1982) 343; A.H. Chamseddine, A. Arnowitt, P. Nath, Phys. Rev. Lett. 49 (1982) 970; L.J. Hall, J. Lykken, S. Weinberg, Phys. Rev. D 27 (1983) 2359.
- [9] <http://www.physto.se/~edsjo/darksusy/>
- [10] <http://www.lpm.univ-montp2.fr:7082/~kneur/suspect.html>
- [11] M. Knecht, A. Nyffeler, Phys. Rev. D 65 (2002) 073034; M. Knecht et al. Phys. Rev. Lett. 88 (2002) 071802.
- [12] C. Le Mouél, Phys. Rev. D 64 (2001) 075009; C. Le Mouél, Nucl. Phys. B 607 (2001) 38.
- [13] J.L. Feng, K.T. Matchev, T. Moroi, Phys. Rev. Lett. 84 (2000) 2322; Phys. Rev. D 61 (2000) 75005; J.L. Feng, K.T. Matchev, F. Wilczek, Phys. Lett. B 482 (2000) 388.
- [14] J.R. Ellis, K.A. Olive, Phys. Lett. B 514 (2001) 114.
- [15] J.L. Silverd et al., astro-ph/0205387.
- [16] M. Urban et al., Phys. Lett. B 293 (1992) 149.
- [17] G. Jungman et al., Phys. Rept. 267 (1996) 195-373.
- [18] L. Bergstrom, Rep. Prog. Phys. 63 (2000) 793.

- [19] K.Griest, D.Seckel, Phys. Rev. D 43 (1991) 3191.
- [20] L.Roszkowski, R.Ruiz de Austri, T.Nihei, JHEP 0108:024 (2001). See also, H.Baer, M.Brulik, Phys. Rev. D57 (1998) 567; A.Corsetti, P.Nath, Int. J. Mod. Phys. A 15 (2000) 905; A.Bottino et al., Phys. Rev. D 63 (2001) 125003; A.B.Lahanas, D.V.Nanopoulos, V.C.Spanos, Phys. Rev. D 62 (2000) 023515; A.Djouadi, M.Drees, J.L.Kneur, JHEP 0108 (2001) 055.
- [21] E.W.Kolb, M.Turner, The Early Universe (Addison-Wesley).
- [22] M.Srednicki, R.Watkins, K.Olive, Nucl. Phys. B 310 (1988)693.
- [23] M.Battaglia et al., Eur.Phys.J. C24 (2002) 311-322.
- [24] J.Ellis et al., Eur.Phys.J. C24 (2002) 311-322.
- [25] L.Bergstrom et al., Astropart.Phys. 9 (1998) 137-162.
- [26] M.de Naurois, et al. 2002, ApJ 566, 343.
- [27] J.Holder, for the CELESTE collaboration 2001, High-Energy Gamma-Ray Astronomy (Heidelberg), AIP Conf. Proc. 558, ed. F.A.Aharonian & H.J.Voelk, 635.
- [28] R.Le Gallou, 2001, Ph.D. Thesis, University of Orsay-Paris XI.
- [29] S.Ghigna et al., 1998, MNRAS 300, 146.
- [30] A.Klypin et al., ApJ 522, 82.
- [31] V.Springel et al., 2001, MNRAS 328, 726.
- [32] B.Moore et al., 1999, MNRAS, 310, 1147.
- [33] F.Stoehr et al., astro-ph/0203342.
- [34] N.Dalal, C.S.Kochanek, 2001 astro-ph/0111456.
- [35] P.Blasi, R.K. Sheth 2000, Phys. Lett. B 486, 233.
- [36] E.Hayashi et al., 2001, astro-ph/0203004.
- [37] P.Coté et al., 2002, astro-ph/0203410.
- [38] E.Giraud et al., 2002, to appear in ESO-ESA-CERN Conference, Garching 4-7 March 2002.

- [39] G.Tóth, J.P.Ostriker 1992, ApJ 389, 5.
- [40] H.Velázquez, S.D.M.White 1999, MNRAS 304, 254.
- [41] E.Ardi, T.Tsuchiya, A.Burkert 2002, astro-ph/0206026.
- [42] A.Font et al., 2001, ApJ 563, L1.
- [43] C.Calcanéo-Roldán, B.Moore, Phys.Rev. D62 (2000) 123005.
- [44] F.Stoehr, S.D.M.White, private communication.
- [45] T. Baltz, et al., Phys.Rev.D61:023514,2000.
- [46] P. Salati, Nucl.Phys.Proc.Suppl.87:366-376,2000 TAUP 99.
- [47] R.Bacon et al. ,2001, astro-ph/0010567.
- [48] T.S.Statler et al., 1999, AJ, 117, 89.
- [49] J.Maggorian, S.Tremaine 1999, M.N.R.A.S 309, 447.
- [50] P.Gondolo, J.Silk 1999, Phys. Rev. Lett. 83, 1719.
- [51] P.Ullo, Zhao HongSheng, M.Kamionkowski, 2001, Phys.Rev. D64 (2001) 043504.
- [52] D.Merritt, et al., 2002, Phys. Rev. Lett., 88 (2002) 191301.
- [53] V.Springel, N.Yoshida, S.D.M.White 2001, New Astronomy 6,79.
- [54] J.F.Navarro, M.Steinmetz, 2000, ApJ, 528, 607.
- [55] J.A.Sellwood, 2000, ApJL, 540, L1.
- [56] W.J.G.de Blok et al., 2001, ApJL, 552, L23.
- [57] C.Carignan, 1999, in New Extra-galactic Perspectives in the New South Africa, eds. D.L.Blok & J.M.Greenberg (Dordrecht: Kluwer), 447.
- [58] D.Pfenniger, F.Combes, 1994, A & A, 285, 94.
- [59] J.A.Irwin, L.M.Widrow, J.English, 2000, ApJ, 529, 77.
- [60] E.Giraud, 2001, ApJ, 558, L23.